Exp Fluids (2007) 42:363–369
DOI 10.1007/s00348-006-0242-6

RESEARCH ARTICLE

Lift-induced drag of a cambered wing for $Re \leq 1 \times 10^6$

P. Gerontakos · T. Lee

Received: 29 June 2006 / Revised: 23 November 2006 / Accepted: 29 November 2006 / Published online: 24 December 2006

Abstract An investigation of the dependence of the lift-induced drag coefficient C_{Di} of a square-tipped, cambered wing model on Reynolds number for $Re \leq 1 \times 10^6$ was conducted. Computed based on the vorticity distribution inferred from the near-field cross-flow velocity measurements of the tip vortex, different C_{Di} prediction schemes were used. The effect of measurement plane size and grid resolution on the C_{Di} calculations was also identified. The C_{Di} estimated by the integral method was found to increase with increasing Re and was below the $C_{Di} = C_l^2/\pi e\mathrm{AR}$ prediction. Limits on the measurement plane size and grid resolution were determined to be at least 40% larger than the vortex outside diameter and no larger than 0.63% chord, respectively, in order to provide a good estimate of the induced drag.

List of symbols

AR	aspect ratio, $= b^2/S$
b	semi-wing span
c	chord
C_{Di}	induced drag coefficient $= D_i/\frac{1}{2}\rho u_\infty^2 S$
C_l	lift coefficient
D_i	lift-induced drag
e	span efficiency factor
M_∞	freestream Mach number
r	radial position
r_c	vortex core radius
r_o	vortex outer radius
Re	Reynolds number, $= u_\infty c/\nu$
S	wing area
t_{max}	maximum airfoil thickness
u, v, w	axial, transverse and spanwise velocities
u_∞	free-stream velocity
v_θ	tangential velocity
x, y, z	streamwise, transverse and spanwise directions
ζ	streamwise vorticity
Γ	circulation or vortex strength
Γ_b	bound circulation
Γ_c	core circulation
Γ_o	total circulation
α	angle of attack
ψ	stream function
ϕ	velocity potential
ρ	fluid density
ν	kinematic viscosity
σ	a source term in Eq. 2

P. Gerontakos · T. Lee (✉)
Department of Mechanical Engineering, McGill University,
817 Sherbrooke St. W., Montreal, QC, Canada H3A 2K6
e-mail: tim.lee@mcgill.ca

1 Introduction

The lift-induced drag generated by aircraft wingtip vortices, because of its undesirable impact on the aerodynamic efficiency, continues to be of concern to the aviation industry and aircraft manufacturers alike. The recent winglet retrofit order of Southwest Airline for 169 737-700/800, capable of saving 92,000 gallons of fuel per year per aircraft (Aviation Week and Space Technology 2003), further reinforces the paramount importance of the wingtip vortex-induced drag and its

control. Extensive research efforts have been devoted to measure and predict the characteristics of the trailing vortices. However, despite much work on the characterization and control of the tip vortex flow, the values of the lift-induced drag were generally not reported. Birch and Lee (2004) computed the lift-induced drag coefficient C_{Di}, based on vorticity inferred from the measured near-field cross-flow velocity field of the tip vortex, through application of the Maskell wake-integral method (Maskell 1973) at different downstream distances behind a NACA 0015 half-wing model with an aspect ratio AR of 2.5 for $\alpha = 8^{\circ}$ and $Re = 1.41 \times 10^5$. The C_{Di} computed was found to be insensitive to x/c and was considerably smaller than that predicted by Prandtl's simple expression

$$C_{Di} = C_l^2/\pi e \mathrm{AR} \quad (1)$$

Gold and Visser (2002) estimated the value of C_{Di} for a swept and tapered NACA 0012 semi-wing with AR = 5.33 at $Re = 1.25 \times 10^5$ by using the wake integral method; a C_{Di} of 0.0082 at $C_l = 1.0$, compared to $C_{Di} = 0.0305$ predicted by Eq. 1, was obtained. Similar C_{Di} results were also reported by Gerontakos and Lee (2006) by using a swept and tapered NACA 0015 wing model at $Re = 1.81 \times 10^5$. Brune (1994) and Kusunose (1997, 1998) reported a C_{Di} of 0.01412 which is 20% lower than $C_{Di} = 0.01773$ predicted by Prandtl's simple expression, based on the measured trailing wake at one chord length behind the trailing edge of a NACA 0016 wing of AR = 6 at $\alpha = 8.2^{\circ}$ with $C_l = 0.5723$ for $Re = 1.27 \times 10^6$. On the other hand, Cummings et al. (1996) computed numerically the C_{Di} of an elliptic wing with an AR of 7 at $M_\infty = 0.5$ and $\alpha = 4^{\circ}$ and found that the C_{Di} computed value is within 1% of the value predicted by Eq. 1. In summary, it is known that Eq. 1 is generally applied to thin airfoils (with $t_{max} \le 12\%c$ and at small angles of attack) in high-speed flows with inviscid assumptions, and that a discrepancy between the C_{Di} values estimated by the integral method and Eq. 1 was observed at low Reynolds numbers. A survey of the C_{Di} variation with Re (for $Re \le 1 \times 10^6$) is therefore needed.

The main objective of the present experiment was to examine the variation of C_{Di}, estimated by various C_{Di} prediction schemes, with Re for $Re \le 1 \times 10^6$ of a thin cambered semi-wing with a fixed AR. Wind-tunnel force balance data were also obtained to supplement the lift-induced drag determinations. The effects of measurement grid size and plane size on the induced drag were also examined. The behavior of the near-field tip vortex flow and the core parameters, measured with a miniature seven-hole pressure probe, as functions of Re were also documented and discussed.

2 Experimental apparatus and methods

The experiment was conducted in the recently constructed $0.9 \times 1.2 \times 2.7$ m suction-type subsonic wind tunnel at McGill University with a free-stream turbulence intensity of 0.03% at a freestream velocity u_∞ of 10 m/s. A square-tipped, rectangular high-lift cambered R and D wing model with a chord c of 50.8 cm, a maximum thickness t_{max} of 10%, a maximum camber of 1.5%c and an effective AR of 1.5 was used as the test model (Fig. 1a). The wing model was mounted vertically at the center of the bottom wall of the wind tunnel test section. The origin of the coordinate system was located at the leading edge of the wing tip. Mean tip-vortex flow velocities (u, v and w) were measured in a plane perpendicular to the free-stream velocity at $x/c = 2.0$ for $\alpha = 6^{\circ}$ by using a miniature seven-hole pressure probe with an outside diameter of 2.6 mm. Eight pressure transducers (seven for the probe and one for tunnel reference total pressure) were used to maximize the data rate of the probe measurement system at each measurement location. The pressure signals were sampled at 500 Hz with a sampling time of 5 s, and were recorded on a PC through a 16 bit A/D converter board. Probe traversing was achieved through a custom-built computer-controlled traversing system. The measurement plane had 56×93 measuring grid points consisting of both a course increment of $\Delta y = \Delta z = 6.4$ mm and a finer $\Delta y = \Delta z = 3.2$ mm (equivalent to 6.3%t_{max} or 0.63%c) which was used in the tip vortex flow region to maximize the accuracy of the vorticity computation as well as the determination of the vortex core parameters. Figure 1b shows the adaptive grid method employed in the present experiments. Note that due to the limitation of the probe traversing mechanism, the present wake survey region only encompassed 93% of the entire wing. The blockage ratio caused by the wing model was less than 4%. Seven chord Reynolds numbers ranged between 2.50×10^5 and 1.0×10^6 were tested. For lift and drag measurements, the finite wing model was mounted vertically on an external two-component force balance located below the wind tunnel. The maximum experimental uncertainties in the results reported have been estimated to be (Gerontakos and Lee 2006): mean velocity 3.5%, vorticity component 8%, vortex radius 4%, and velocity fluctuation 3%. The uncertainty in lift coefficient and C_{Di} were ± 0.01 and 5%, respectively.

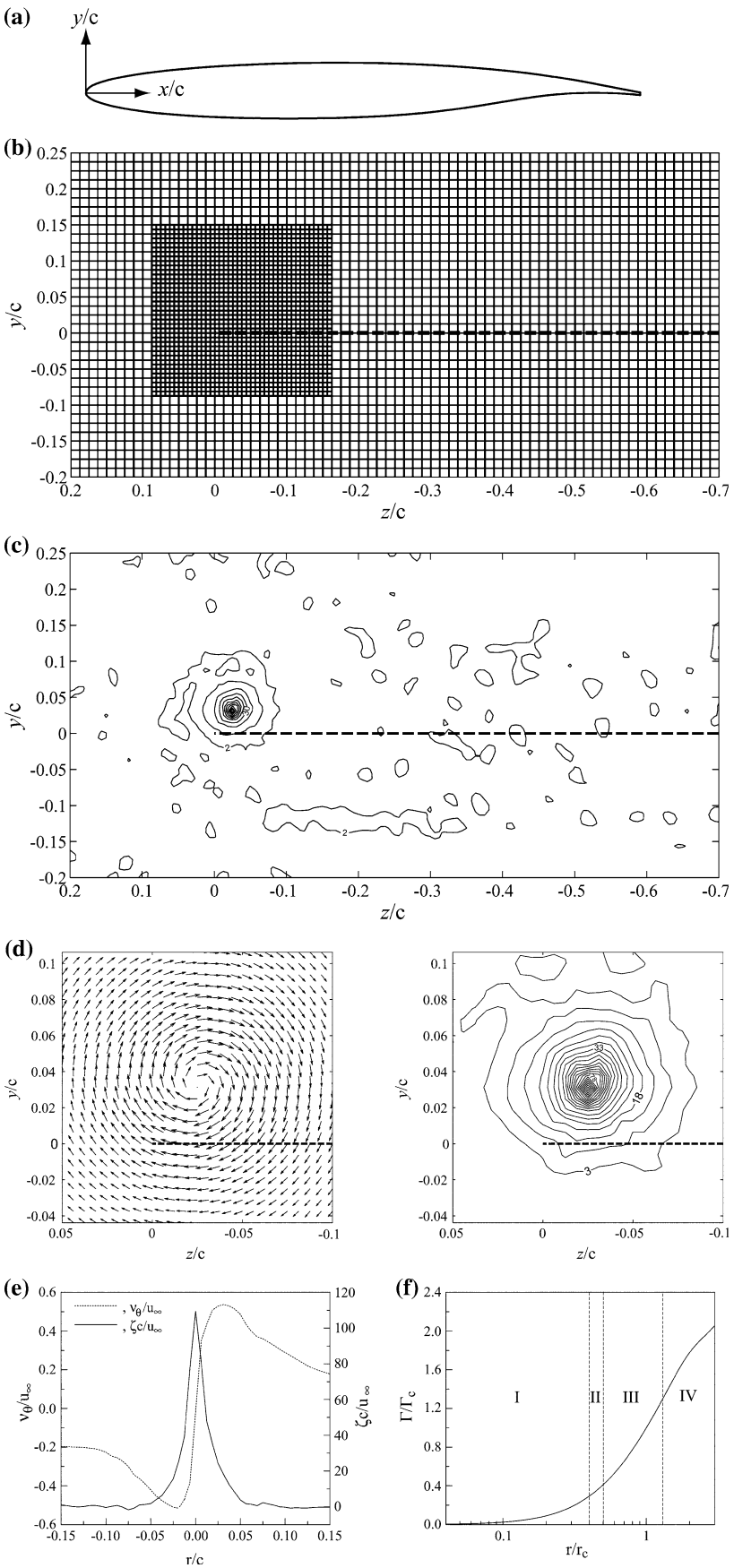

Fig. 1 **a** Wing model profile, **b** adaptive measurement grid, and **c** normalized iso-vorticity contours for $Re = 5.01 \times 10^5$. The *dashed line* indicates the wing trailing edge. **d** Normalized mean vw-velocity vectors and streamwise iso-vorticity contours, **e** tangential velocity and vorticity distributions across the vortex center, and **f** behaviour of radial circulation for $Re = 501{,}000$. Numerical values denote $\zeta c/u_\infty$ level with constant increment of 5.0. I: Inner-core region, II: buffer region, III: logarithmic region, and IV: outer region

3 Results and discussion

3.1 Typical vortex flow characteristics

The Reynolds number dependence of the measured near-field tip vortex flowfield is characterized first as it dominates the magnitude of C_{Di}. Figure 1c presents the typical non-dimensional streamwise iso-vorticity $\zeta c/u_\infty$ contours over the entire wake for $Re = 5.01 \times 10^5$ at $x/c = 2$; the majority of the vorticity was concentrated in the tip vortex flow region. For clarity, the vw-velocity vector plot and $\zeta c/u_\infty$ contour were reproduced and are presented in Fig. 1d, which clearly indicate the axisymmetry of the inner flow of the vortex, suggesting a near completion of the shear layer roll-up. The corresponding tangential v_θ and ζ distributions across the vortex center are shown in Fig. 1e. It is also of interest to note that the nearly axisymmetric tip vortex flow can also be demonstrated from the self-similar behavior (a characteristic of a far wake) observed in the radial circulation distribution $\Gamma(r)$ in the near field of a vortex generator. The tip vortex core was found to follow an $\Gamma \propto r^2$ profile for $r/r_c < 0.4$ and vary logarithmically for $0.5 < r/r_c < 1.4$ (Fig. 1f). r_c is the core radius defined by the location of $v_{\theta peak}$. The circulation was calculated by employing Stokes' theorem (i.e. a surface integration of the vorticity). For $r/r_c > 1.4$, $\Gamma(r)$ continued to vary with r, suggesting that there was a slow addition of vorticity (as much as 15% of the bound circulation Γ_b; Gerontakos and Lee 2006) to the outer layers of the vortex from the shear layer arriving from the inboard regions. The asymptotic limits to the formal expressions derived by Hoffman and Joubert (1963) and Phillips (1981) to describe the circulation field in the core region are $\Gamma(r)/\Gamma_c = 1.44(r/r_c)^2$ and $\Gamma(r)/\Gamma_c = 2.27 \log(r/r_c) + 1.0$ for $r/r_c < 0.4$ and $0.5 < r/r_c < 1.4$, respectively, for the Re tested. The influence of Re on the vortex core parameters was also examined and is summarized in Fig. 2.

Figure 2a, b show that there was a gradual and minor increase in $v_{\theta peak}/u_\infty$, accompanied by a reduction in r_c, with Re, as a result of the observed reduction in Γ_c with Re, for $Re \le 6.68 \times 10^5$ (Fig. 2c); an average $v_{\theta peak}$ of about $0.54u_\infty$ and $r_c \approx 0.027c$ was observed for the Re range tested. The peak vorticity ζ_{peak}/cu_∞, however, increased nonlinearly with increasing Re for $Re \le 6.68 \times 10^5$. The outer radius r_o (obtained by measuring the extent as the circulation $\Gamma(r_o)$ reached 98% of the total circulation Γ_o) was found to increase considerably with Re for $Re < 4.17 \times 10^5$, while remaining virtually unchanged at $r_o \approx 0.09c$ for $Re \ge 4.17 \times 10^5$ (Fig. 2b). More importantly, the present measurements also reveal that both Γ_o and Γ_b were also found to remain constant with $\Gamma_o/cu_\infty = 0.16$ and $\Gamma_b/cu_\infty = 0.188$, which translates into a $\Gamma_o/\Gamma_b \approx 85\%$; i.e. nearly 85% of the bound circulation was entrained into the near-field tip vortex at $x/c = 2.0$ for Re tested. This observation is of importance in the justification of the subsequent C_{Di} determination via the near-field tip vortex flow measurements. Details of the physical behavior of the near-field core flow parameters are given in Birch and Lee (2004) and Gerontakos and Lee (2006).

3.2 Lift-induced drag

The lift-induced drag coefficient C_{Di} at $\alpha = 6^\circ$ for $Re \le 1.0 \times 10^6$ was computed using the Maskell induced-drag model. The vw-crossflow velocity vectors within the measurement plane at $x/c = 2.0$ were decomposed into a stream function $\psi(y, z)$ and a crossflow velocity potential $\phi(y, z)$ with the imposed boundary conditions requiring both ψ and $\partial\phi/\partial n = 0$ to be zero on the walls of the wind tunnel. The lift-induced drag D_i (Brune 1994; Kusunose 1997, 1998) was then obtained by

$$D_i = 1/2\ \rho_\infty \iint_{S\zeta} \psi\zeta\, dy\, dz - 1/2\ \rho_\infty \iint_{S1} \varphi\sigma\, dy\, dz - 1/2\ \rho_\infty \iint (1 - M_\infty^2)(\Delta u)^2 dy\, dz \quad (2)$$

where ζ ($= \partial w/\partial y - \partial v/\partial z$) is the streamwise vorticity, the surface S_ζ is the region within S1 where the vorticity is nonzero, σ ($= \partial v/\partial y + \partial w/\partial z = -\partial u/\partial x$) is a source term which is small outside the viscous wake. Note that the third integral was introduced by Betz (1925) and is usually assumed to be negligible. The stream function and velocity potential were determined in two ways. The first scheme used the velocity field by solving the following two equations at each measurement location: $v = \partial\psi/\partial z + \partial\phi/\partial y$ and $w = -\partial\psi/\partial y + \partial\phi/\partial z$. This was done via a centered finite difference computational scheme, by letting $2\Delta s v_{j,i} = -\psi_{j,i-1} + \psi_{j,i+1} - \phi_{j-1,i} + \phi_{j+1,i}$ and $2\Delta s w_{j,i} = \psi_{j-1,i} - \psi_{j+1,i} - \phi_{j,i-1} + \phi_{j,i+1}$, for a given data set with uniform grid points (i.e. $\Delta y = \Delta z = \Delta s$). The second scheme solved the Poisson equations: $\partial^2\psi/\partial y^2 + \partial^2\psi/\partial z^2 = -\zeta$ and $\partial^2\phi/\partial y^2 + \partial^2\phi/\partial z^2 = \sigma$; again using a centered finite difference computational scheme. It is of note that solving the Poisson equations for $\psi(y, z)$ and $\phi(y, z)$ required less computational time and yielded slightly improved results, within measurement error, than solving for them from the velocity fields.

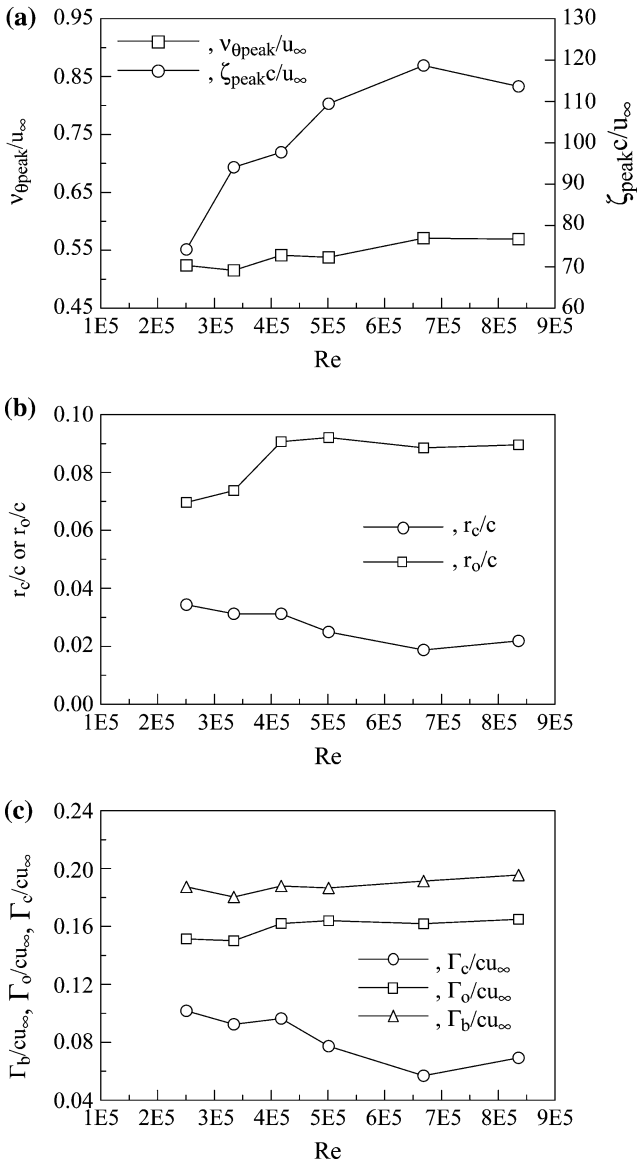

Fig. 2 Critical vortex flow parameters

Figure 3 shows the variation of the magnitude of C_{Di} (denoted by Δ symbols) for $\Delta y = \Delta z = 3.2$ mm or 0.63%c with *Re*. A general increase in C_{Di} was observed with increasing *Re*, as a result of thinning of the boundary layer, resulting in a further delay in the trailing-edge flow separation and increased lift. Also shown in Fig. 3 are the C_{Di} values (denoted by circles) estimated by using Eq. 1 with C_l values obtained through a force balance. A large difference (as much as 25%) existing in the C_{Di} values determined by Eq. 2 and Eq. 1 was observed. The Prandtl's simple expression, which is frequently employed in high Reynolds number or intuitively inviscid flow conditions, was found to provide an upper bound of C_{Di} estimation for low-*Re* flows in which the viscous effects become

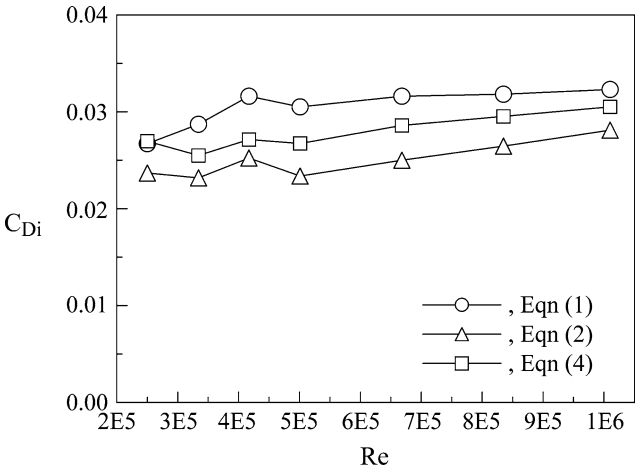

Fig. 3 Lift-induced drag coefficient

dominant and trailing-edge flow separation is unavoidable. Moreover, since the $C_{Di} = C_l^2/\pi eAR$ prediction is dominated by the magnitude of C_l, the accuracy of the C_l values determined with a force balance was checked against the C_l obtained indirectly from the integral of the spanwise circulation $\Gamma(z)$ distribution; i.e. $L = \rho_\infty u_\infty \int_{-b/2}^{b/2} \Gamma(z)dz = \rho_\infty u_\infty \iint \zeta\, z dy\, dz$. The lift coefficient computed was found to be in good agreement with those obtained directly with a force balance (Fig. 4a). Additionally, the present whole wake measurements also indicate that no significant difference in the normalized $\Gamma(z)$ distributions in the near field with *Re*, especially in the tip region, was observed (Fig. 4b). A precipitous dip in the spanwise $\Gamma(z)$ distribution near the tip (Gerontakos and Lee 2006), however, was observed, suggesting that the rectangular wing had a tip vortex of stronger vortex strength and higher lift-induced drag compared to an elliptic wing at the same α.

It is also noteworthy that although the application of the Maskell formulation of the lift-induced drag is straight forward and very advantageous since only the viscous wake is required to be measured, the computation of $\psi(y, z)$ and $\phi(y, z)$, however, makes it extremely computationally intensive and could therefore suffer from reduced versatility. In addition, the two boundary conditions required in solving for ψ and ϕ demand that the wind-tunnel walls are a stream function with $\psi = 0$, and that there is no flow across the tunnel wall (i.e. $\partial\phi/\partial n = 0$). As a result, even though the crossflow measurements are confined to a small region of the tunnel test section, a computational grid encompassing the entire test section is still required so as to implement the imposed above-mentioned boundary conditions. Consequently, if the measurements are conducted at reasonably high resolution, this

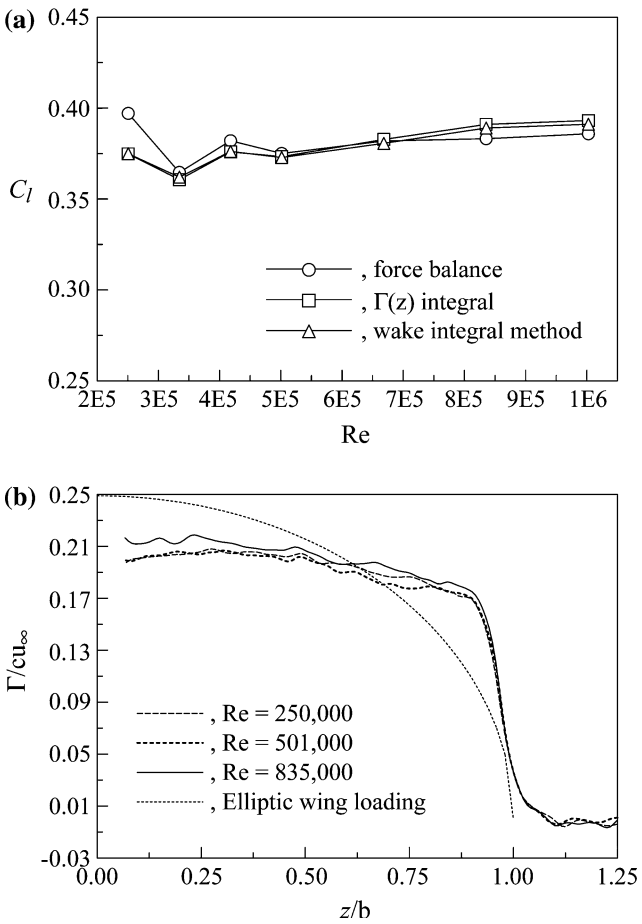

Fig. 4 **a** C_l and **b** spanwise circulation distribution

results in a large number of grid points when solving for $\psi(y, z)$ and $\phi(y, z)$, which would prohibit a PC from completing the calculations. Nevertheless, the integral expressed in Eq. 2 is still very attractive due to the fact that the vorticity is nonzero in only a limited area of the crossflow plane so that the integration can be performed over a finite region (as discussed later in Fig. 6), and that the values of this integral are fairly insensitive to the streamwise location of the plane on which they are evaluated.

An alternative way of determining the stream function by using Green's function to solve the Poisson equation analytically (Cummings et al. 1996; Kusunose 1997, 1998; Kusunose and Crowder 2002) was also employed. Note that the calculation of induced drag by making use of Green's function does not require an extension of the computational area to the entire test section and as a result is extremely more computationally efficient. By relating the crossflow vorticity to the local circulation and replacing differentiation with integration (which alleviates the uncertainty associated with the direct differentiation of the discrete velocity measurements), the

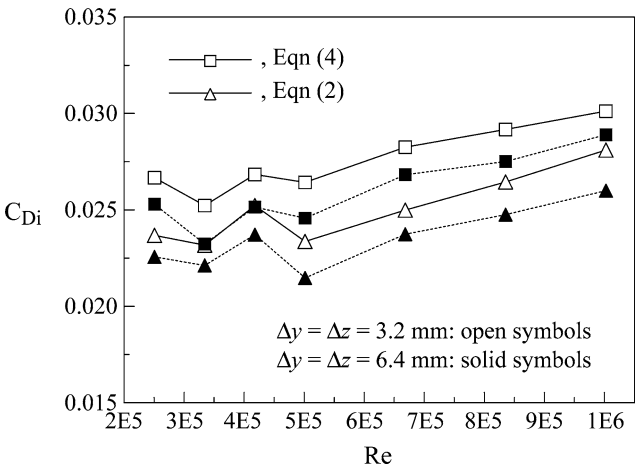

Fig. 5 Effect of grid size on C_{Di}

streamwise component of vorticity in each measurement cell can be approximated by $\zeta_{j+½,k+½} = \Gamma_{j+½,k+½}/\Delta y\Delta z$ and $\Gamma_{j+½,k+½} = ½(v_{j,k} + v_{j+1,k})\Delta y + ½(w_{j+1,k} + w_{j+1,k+1})\Delta z - ½(v_{j+1,k+1} + v_{j,k+1})\Delta y - ½(w_{j,k+1} + w_{j,k})\Delta z$. $v_{j,k}$ and $w_{j,k}$ are the crossflow velocity components. The stream function (for an arbitrary distribution of vorticity) is $\psi(y, z) = -(1/4\pi)\iint\zeta(y_o, z_o)\log[(y - y_o)^2 + (z - z_o)^2]dy_o dz_o$ with the integral being approximated by using the formulation described by Lamb (1932),

$$\begin{aligned}\psi_{j,k} &= -\left(1/4\pi\right)\sum_{j_o,k_o}\Delta y\Delta z\zeta_{j_o+1/2,k_o+1/2}\\ &\quad\times\log\left[(j_o+1/2-j)^2\Delta y^2+(k_o+1/2-k)^2\Delta z^2\right]\\ &= -\left(1/4\pi\right)\sum_{j_o,k_o}\Gamma_{j_o+1/2,k_o+1/2}\\ &\quad\times\log\left[(j_o+1/2-j)^2\Delta y^2+(k_o+1/2-k)^2\Delta z^2\right]\end{aligned} \tag{3}$$

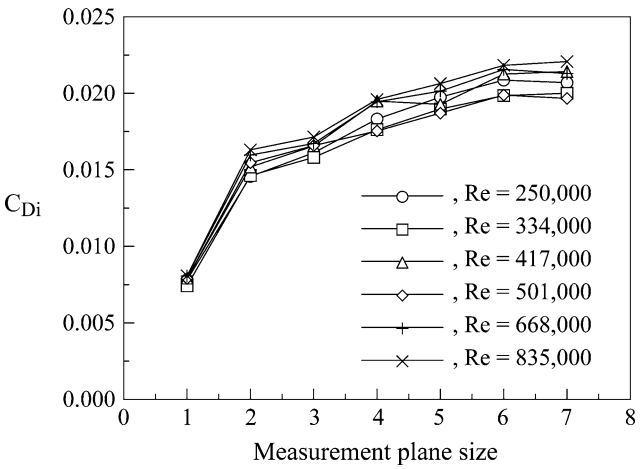

Fig. 6 Effect of measurement plane size on C_{Di}

The drag integral is thus approximated by summing over each cell to give the induced drag as

$$D_i = 1/2\ \rho_\infty \sum_{j,k} 1/4\ \left(\psi_{j,k} + \psi_{j+1,k} + \psi_{j,k+1} + \psi_{j+1,k+1}\right)\Gamma_{j+1/2,k+1/2} \quad (4)$$

Note that the calculation of $\psi(y, z)$ is based on the "left half-wake" case as described by Kusunose (1998). Figure 3 shows that while the C_{Di} determined by Eq. 4 (denoted by square) was only about 5% higher than those computed by the wake integral method (i.e. Eq. 2), the computational complexity and time required were, however, substantially reduced.

In addition, it is known that the wing-tip vortex flow region contains the steepest vw-velocity gradients and the concentrated vorticity distribution (as shown in Fig. 1c, d), therefore it dominates the magnitude of the induced drag. Three different measurement grid sizes (Δs = 1.6, 3.2, and 6.4 mm equivalent to 0.315, 0.63, and 1.26%c) were considered for each of the Reynolds number tested. Figure 5 shows an increase in grid resolution (i.e. with Δs = 3.2 mm) improved the C_{Di} calculation by 5–8% and 6–9% by the use of Eqs. 2 and 4, respectively. No noticeable improvement in the estimates of C_{Di} values were noticed for 1.6 mm grid size compared to those obtained with Δs = 3.2 mm.

Finally, the effects of seven different measurement plane sizes, comparable to the outer diameter of the tip vortex (as shown in Fig. 2b), on the accuracy of the lift-induced drag were investigated for a uniform grid size of 3.2 mm. The smaller plane sizes S_3 (= $1.4r_o \times 1.4r_o$) and S_4 (= $2.1r_o \times 2.1r_o$) were chosen to enclose the entire tip vortex flow region (i.e. $S_2 = 1.0r_o \times 1.0r_o$) while remained comparable to it. Plane sizes S_5 to S_7 (= $2.6r_o \times 2.8r_o$, $2.6r_o \times 3.91r_o$ and $2.6r_o \times 5.02r_o$) were selected to reflect the influence of the incremental inclusion of the wake portion on the C_{Di} value. Figure 6 indicates that the magnitude of C_{Di} was generally increased with the plane size (except the dip observed in the measurement plane size S_5 for $Re = 4.17 \times 10^5$). No noticeable difference in value of C_{Di} was observed between scan sizes S_6 and S_7, while a 5–10% reduction in value was observed for each reduction in scan size for S_2, S_3, S_4, and S_5 (compared to plane sizes S_6 and S_7). The smallest plane size $S_1 = 0.5r_o \times 0.5r_o$ led to a substantially underestimated C_{Di} value. In conclusion, it is shown that the trailing wake, excluding the concentrated tip vortex region, only contributed about 20% to the total C_{Di} value and a measurement plane size at least 40% larger than the outer diameter of the tip vortex is needed to provide a reasonably accurate estimate of the C_{Di} value.

4 Conclusions

The lift-induced drag coefficient C_{Di}, computed based on the near-field vorticity distribution inferred from the measured cross-flow velocity of a tip vortex, of a square-tipped cambered wing model positioned at $\alpha = 6^\circ$ for $Re \le 1 \times 10^6$ was obtained. The evolution of the tip vortex flow was found to be nearly complete, especially in the inner region of the vortex flow, in the near field behind the wing tip. For the low-Reynolds number flows tested, the C_{Di} was found to generally increase with Re and was of lower values (as much as 25%) than those estimated by using the simple inviscid $C_{Di} = C_l^2/\pi e$AR expression. Also, by relating the crossflow vorticity to the local circulation and replacing the differentiation with integration, the C_{Di} value can be obtained with a considerably reduced computational time, while the accuracy, within measurement error, remained about the same. A maximum measurement grid size of 0.63% chord and a plane size larger than 40% of the outside diameter of the vortex are needed to provide a good estimate of the C_{Di}.

References

Aviation week and space technology (2003) June 23, p 15

Betz A (1925) A method for the direct determination of profile drag. ZFM 16:42–44

Brune GW (1994) Quantitative low-speed wake surveys. J Aircr 31(2):249–255

Cummings RM, Giles MB, Shrinivas GN (1996) Analysis of the elements of drag in three-dimensional viscous and inviscid flows. AIAA-96-2482

Birch D, Lee T (2004) The structure and induced drag of a tip vortex. J Aircr 41(5):1138–1145

Gerontakos P, Lee T (2006) Near-field tip vortex behind a swept and tapered wing model. Exp Fluids 40:141–155

Gold N, Visser K (2002) Aerodynamic effects of local dihedral on a raked wingtip. AIAA-2002-0831

Hoffmann ER, Joubert PN (1963) Turbulent line vortices. J Fluid Mech 16:395–411

Kusunose K (1997) Development of a universal wake survey data analysis code. AIAA-97-31757

Kusunose K (1998) Drag prediction based on a wake-integral method. AIAA-98-2723

Kusunose K, Crowder JP (2002) Extension of wake-survey analysis method to compressible flows. J Aircr 36(9):954–963

Lamb H (1932) Hydrodynamics. 6th edn. Cambridge University Press, Cambridge, pp 219–220, 592

Maskell E (1973) Progress towards a method for the measurement of the components of the drag of a wing of finite span. RAE Technical Report 72232

Phillips WRC (1981) The turbulent trailing vortex during roll-up. J Fluid Mech 105:451–467